Demonstration of Pattern Division Multiple Access with Message Passing Algorithm in MMW-RoF Systems

Shuyi Shen, You-Wei Chen, Qi Zhou, and Gee-Kung Chang
Georgia Institute of Technology, Atlanta, GA 30332 USA
ssyzoe@gatech.edu

Abstract: Implementing PDMA with MPA, ambiguous symbol recovery and 4-dB sensitivity improvement was achieved compared to conventional PD-NOMA-SIC. Experimental results show that PDMA enhances application flexibility by pattern variants tailored for different scenarios including grant-free uplinks.

OCIS codes: (060.5625) Radio frequency photonics; (060.2330) Fiber optics communications

1. Introduction

Pattern division multiple access (PDMA) is a novel non-orthogonal multiple access (NOMA) scheme that has been discussed and investigated for fifth-generation (5G) radio access networks (RAN) [1,2]. In a 5G MMW small cell as shown in Fig. 1(a), users served by one remoted radio unit (RRU) can have different channel qualities: users with good line-of-sight links (user equipment 1, UE1, with channel 1, CH1); edge users far away from RRU experiencing low signal-to-noise ratio (SNR) and channel gain due to high MMW path loss (UE2 with CH2); or users suffering severe channel degradation (UE3 with CH3) caused by MMW links susceptible to blockage, antenna misalignment, etc. With such disparate reception qualities, RRU implementing conventional orthogonal frequency-division multiple access (OFDMA) has to sacrifice spectral efficiency to serve low-SNR users with low QAM orders [3]. To solve the issue, NOMA is proposed and investigated for next-generation RAN to fully utilize channel capacity by exploiting power domain multiplexing for multiple user access. PDMA is one of the promising NOMA candidates. In addition to power-domain NOMA (PD-NOMA), PDMA assigns spreading patterns to differentiate users sharing one time-frequency resource block, as shown in Fig. 1(b) and (c). PDMA pattern matrix defines the third dimension for resource sharing on top of time-frequency resource grids. By customizing the pattern matrix with power scaling and/or phase shifting, PDMA is designed to provide more flexibility in resource allocation.

Another advantage of PDMA is that it facilitates advanced parallel interference cancellation (PIC) at the receiver when the pattern matrix is sparse. In conventional PD-NOMA, successive interference cancellation (SIC) is used, but it is susceptible to error propagation which makes current user decoding highly depend on precedent correctly decoded users. On the other hand, PIC such as message passing algorithm (MPA) with greatly enhanced decoding accuracy can be utilized for PDMA with sparse pattern design. MPA is an approximation of optimum maximum *a posteriori* (MAP) detection based on factor graph, an equivalent representation of a pattern matrix, as shown in Fig. 1(d).

In this paper, PDMA with MPA detection was experimentally demonstrated for the uplink of a MMW radio access network with radio-over-fiber (RoF) mobile fronthaul. Experimental results show that PDMA with MPA can improve sensitivity by 4 dB compared to PD-NOMA with SIC. Moreover, it is experimentally validated that MPA is capable of recovering ambiguous constellation symbols. PDMA with different pattern matrices were also demonstrated and compared. To further validate its flexibility and adaptivity, PDMA with customized power scaling and stream allocation of two users were implemented for different application scenarios. Experimental results show that PDMA is capable of supporting and being adapted to use cases including grant-free uplinks, regular payload uplinks, with comparable and disparate channel conditions.

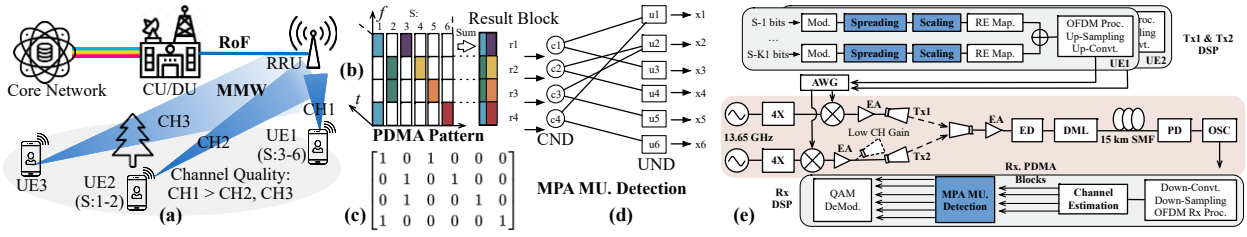

Fig. 1 (a) Schematic diagram of the MMW-RoF system with three users, UE1, UE2 and UE3, experiencing disparate channel quality: CH1, CH2 and CH3, respectively. (b) PDMA resource block. (c) Pattern matrix. (d) MPA factor graph and information passing. (e) Experimental setup.

2. Operating Principles and Experimental Setup

A PDMA matrix supports K streams and their data are mapped onto N resource elements (REs, subcarriers in OFDMA) in accordance with the PDMA pattern as illustrated in Fig. 1(b) and (c). The transmitted symbol vector $\boldsymbol{s}_k$ of stream k is obtained by spreading its modulation symbol x_k according to the PDMA pattern vector $\boldsymbol{g}_k$: $\boldsymbol{s}_k = \boldsymbol{g}_k x_k, 1 \le k \le K$, where $\boldsymbol{s}_k$ is an $N \times 1$ vector [1]. The PDMA pattern matrix for K streams over N REs are $\boldsymbol{G}^{[N,K]} = [\boldsymbol{g}_1, \boldsymbol{g}_2, \ldots, \boldsymbol{g}_K]$ with $\boldsymbol{g}_k$ being an $N \times 1$ vector. An example of PDMA pattern matrix $\boldsymbol{G}_a^{[4,6]}$ is given in Fig. 1(c). Each $\boldsymbol{g}_k$ can be

assigned power scaling and phase shifting by scaling factor α_k. We define the scaling vector as $\boldsymbol{A} = [\alpha_1, \alpha_2, ..., \alpha_K]$. In the experiment, the PDMA patterns were assigned to two users: UE$_1$, and UE$_2$, using transmitter 1 (Tx1) and Tx2, respectively. The transmitted symbol vector for each user is $\boldsymbol{t}_i = \sum_{k \in UE_i} \alpha_k \cdot \boldsymbol{s}_k$, where $\boldsymbol{t}_k$ is an $N \times 1$ vector. In the experiment, all effective subcarriers were divided to groups of resource blocks with size $N \times 1$.

At the receiver (Rx) side, MPA-based multi-user (MU) detection is implemented. Take the PDMA pattern matrix $\boldsymbol{G}_a^{[4,6]}$ as an example, its factor-graph equivalent is shown in Fig. 1(d), consisting of N channel observation nodes (CNDs) and K user (in our case, stream) nodes (UNDs). As an approximation of MAP, information propagates between CNDs and UNDs back and forth until reaching converged inference of x_k. Details of MPA can be find in [4]. In the experiment, quadrature amplitude modulation (QAM)-symbol-level MPA was used for PDMA detection.

Experimental setup of the MMW radio access system with RoF mobile fronthaul is depicted in Fig. 1(e). Two UEs were accessing the RRU via MMW links. K_i PDMA streams in $UE_i = \{S_{i,1}S_{i,2}...S_{i,K_i}\}$ were assigned to each UE$_i$. In the Tx-side digital signal processing (DSP) for each UE$_i$, K_i streams of bits were modulated to QAM symbols. Symbols in each stream used the same QAM order. QAM symbol streams were spread and scaled in accordance with the PDMA pattern matrix and mapped to corresponding REs. The streams of UE$_i$ were then summed and went through traditional OFDM DSP. The subcarrier spacing was $2^7 \times 15kHz = 1.92MHz$, FFT size was 2048, 420 out of which carried the payload, CP length was 1/16 of the symbol duration, the intermediate frequency was 510 MHz, effective signal bandwidth was 806.4 MHz. The digital OFDM signal was converted to analog waveform by an arbitrary waveform generator (AWG, 15.73 GSa/s). At each UE Tx, radio frequency (RF) source generated 13.65 GHz which produced 54.59 GHz carrier frequency after a quadrupler. The AWG output signal was upconverted to the carrier frequency by a mixer. The synthesized MMW signal was then amplified by an electrical amplifier (EA) and transmitted by a horn antenna with 15 dBi. At the Rx side, another horn antenna captured both uplink signals from two UEs. The received signal was down-converted to the baseband by an envelope detector (ED, 1 GHz). The baseband electrical signal was then converted to optical signal by a directly modulated laser diode (DML, 2.5 GHz). After transmission over 15-km standard single-mode fiber (SMF), the signal was captured by a photodetector (PD, 2.5 GHz) and output to an oscilloscope (OSC, 5 GSa/s) for offline DSP. At the Rx, the received signal went through preliminary OFDM demodulation, and channel estimation which was essential for the following MPA detection. Received symbols were divided to resource blocks in accordance with the PDMA pattern matrix. MPA was applied to each received resource block to recover K_i streams of QAM symbols which were then decoded to K_i bit streams for bit-error-rate (BER) calculation.

3. Experimental Results and Discussions

For experimental results shown in Fig. 2(a) and (b), PDMA pattern matrix $\boldsymbol{G}_a^{[4,6]}$ was applied, with $UE_1 = \{1, 4, 5\}$ and $UE_2 = \{2, 3, 6\}$ (defined as benchmark PDMA setting for later experiments), the scaling factor was $\boldsymbol{A} = [-7, -7, 0, 0, 0, 0]dB$, as depicted in Fig. 1(b). In Fig. 2(a), QPSK was applied to stream 1 and 2, 16QAM was applied to stream 3 to 6; in Fig. 2(b), QPSK was applied to all streams. The resulted constellation of Rx signals without channel were plotted in Fig. 2 (a) and (b), respectively. UE$_1$ and UE$_2$ had the same channel gain in this experiment. The power spectrum of the received signal was shown in Fig. 2(c). BER performance of Rx implementing MPA and conventional SIC was compared. Fig. 2(a) and (b) shows the BER of the best and worst streams versus received optical power (RoP) before PD, both in back-to-back (B2B) and over 15-km SMF transmission scenarios. It can be seen that overall MPA-based detection achieved an average 4-dB Rx sensitivity improvement compared to SIC, providing respective1.9-Gbps for both users over 806.4 MHz bandwidth.

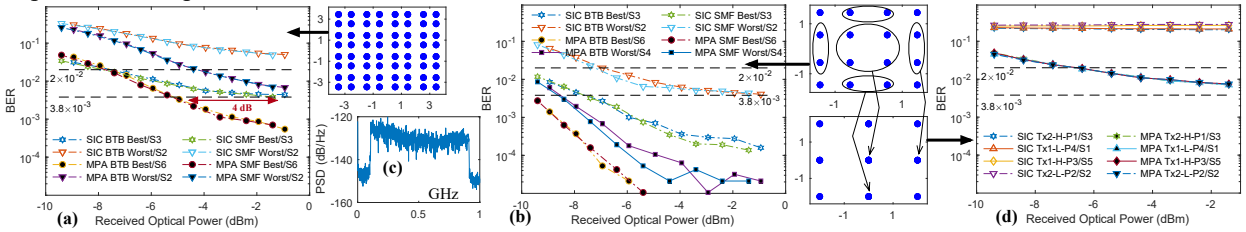

Fig. 2. BER versus RoP of (a)16QAM applied to stream 3 to 6; (b) QPSK applied to stream 3 to 6. (c) Power spectrum of Rx signal. (d) BER versus RoP when constellation ambiguity exists.

Fig. 2(d) shows the PDMA BER performance when there was constellation symbol ambiguity. Fig. 2(d) employed the benchmark PDMA setting with all streams using QPSK and the scaling factor was $\boldsymbol{A} = [0, 0, 0, 0, 0, 0]dB$. In this case, ambiguous constellation symbols existed, as shown in the constellation diagram of Fig. 2(d). For example, for the first received symbol in the resource block as indicated in Fig. 1(b), $r_1 = x_1 + x_3$. (x_1, x_3) pairs such as (1+i, -1-i) and (1-i, -1+i) will both result in $r_1 = 0$. As shown in Fig. 2(d), SIC was not able to differentiate ambiguous symbols

with BER all beyond FEC threshold. While MPA could achieve BER below FEC threshold with high RoP, owing to the fact that inference of x_k is exchanged and shared between CNDs and UNDs in the message passing process.

Different PDMA patterns were also investigated. As shown in Fig. 3(a) and (b), $\boldsymbol{G}_a^{[4,6]}$and $\boldsymbol{G}_b^{[4,6]}$ was applied, respectively. Fig. 3(a) employed the benchmark parameter setting with all streams using QPSK and the scaling factor was $\boldsymbol{A} = [-7, -7, 0, 0, 0, 0]dB$. In Fig. 3(b), $UE_1 = \{1, 2, 3\}$, $UE_2 = \{4, 5, 6\}$, $\boldsymbol{A} = [0, 0, -7, 0, 0, -7]dB$, and QPSK was applied to all streams. Compared to $\boldsymbol{G}_a^{[4,6]}$, in $\boldsymbol{G}_b^{[4,6]}$ each RE was shared by 3 streams instead of 2. As a result, minimum distance of the resulted constellation shrank, degrading overall BER. On the other hand, more inference information was exchanged during MPA process, which improved the detection accuracy for streams with lower assigned power, as demonstrated by the results shown in Fig. 3(b).

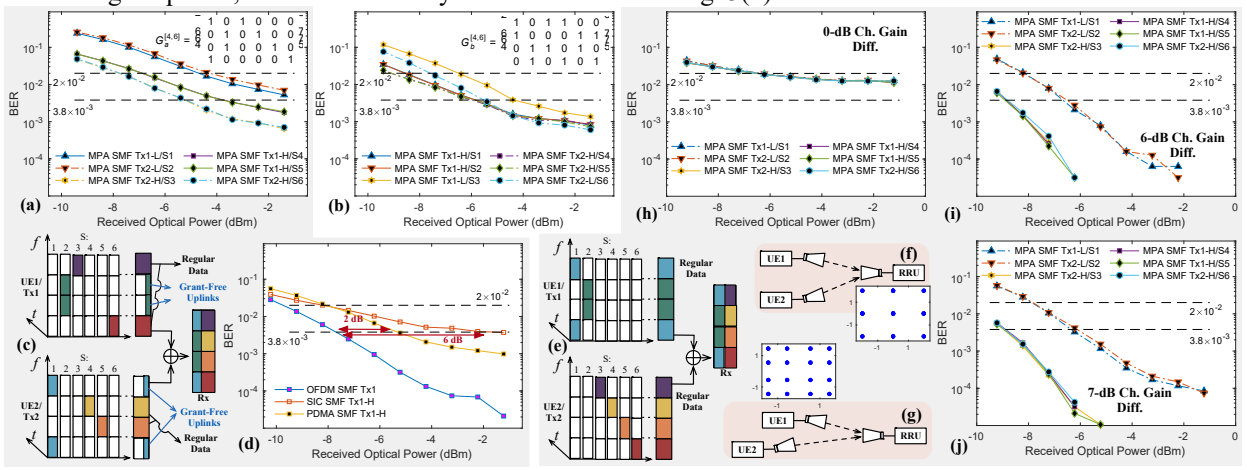

Fig. 3 BER versus RoP for pattern matrix (a) $\boldsymbol{G}_a^{[4,6]}$ and (b) $\boldsymbol{G}_b^{[4,6]}$. (c) PDMA pattern and setting for grant-free uplinks; (d) Penalty compared to conventional OFDM. (e) PDMA pattern and setting for regular uplinks. Transmission scenarios for (f) UE_1 and UE_2 having comparable channel gain and (g) UE_1 having higher channel gain than UE_2. BER performance of $CH\_Gain\{UE_1/UE_2\} =$: (h) 0 dB; (i) 6 dB; (j) 7dB.

As mentioned in Section 1, PDMA utilizes patterns as the third dimension of resource sharing in addition to time-frequency grids, which expands the resource pool, therefore reduces chances of collision in case of contention [1]. Moreover, lower stream power level can reduce the interference to other users sharing the same RE yet maintaining correct detection with powerful MPA. Both factors enable the potential of PDMA supporting grant-free uplinks. Take the benchmark PDMA setting as an example (results shown in Fig. 3(a)), grant-free uplinks were demonstrated. As illustrated in Fig. 3(c), for both UEs, stream 3, 4, 5, 6 were reserved for regular data (16QAM) with high (H) power level, while stream 2 and 1 with low (L) power level (-7 dB) was used for grant-free uplinks (QPSK) of UE_1 and UE_2, respectively, minimizing interference to potential regular users. Experimental results in Fig. 3(a) show that grant-free uplinks (L) provided BER below FEC threshold with RoP > -4 dBm without devastating decoding of regular data streams (H). Penalty brought by PDMA-assisted grant-free uplinks was also measured and plotted in Fig. 3(d). Compared to an interference-free OFDM 16QAM transmission for UE_1, 2-dB sensitivity penalty was brought by MPA-assisted PDMA request-free uplinks, while 6-dB penalty was observed for SIC detection.

To verify the flexibility and adaptivity of PDMA serving regular uplinks, two categories of channel quality scenarios were investigated. In these cases, different power scaling and stream allocation from grant-free uplinks were applied, as depicted in Fig. 3(e), in which $UE_1 = \{1, 2\}$, $UE_2 = \{3, 4, 5, 6\}$, and all streams were assigned the same power scaling factor to fully take the advantages of channel capacity using NOMA. In fact, channel gain serves as 'power scaling' in these cases. Fig. 3(f) and (g) illustrate the two categories of channel quality scenarios tested: 1) UE_1 and UE_2 had comparable channel gain; 2) channel gain of UE_1 was higher than UE_2. Experimental results showing PDMA supporting $CH\_Gain\{UE_1/UE_2\} = \{0, 6, 7\}dB$ are demonstrated in Fig. 3(h), (i), and (j), respectively.

4. Conclusion

PDMA-MPA for MMW radio access system with RoF mobile fronthaul has been demonstrated in this paper. It achieves ambiguous symbol recovery and 4-dB sensitivity improvement in comparison with PD-NOMA-SIC. Different PDMA patterns were also implemented and verified. Experimental results validate the application flexibility of PDMA in supporting grant-free and regular uplinks, with various channel conditions.

5. References

[1] S. Chen et al., in IEEE Transactions on Vehicular Technology, vol. 66, no. 4, pp. 3185-3196, April 2017.
[2] 3GPP TSG RAN WG1, R1-1808386, Gothenburg, Sweden, Aug.20th-24th, 2018.
[3] F. Lu et al., in Journal of Lightwave Technology, vol. 34, no. 17, pp. 4179-4186, 1 Sept.1, 2016.
[4] R. Hoshyar et al., in IEEE Transactions on Signal Processing, vol. 56, no. 4, pp. 1616-1626, April 2008.